

BlindHarmony: “Blind” Harmonization for MR Images via Flow model

Hwihun Jeong, Heejoon Byun, Dong un Kang, and Jongho Lee

Department of ECE, Seoul national university

Seoul, Korea

{hwihuni, ryanb01, qkrtnskfk23, jonghoyi}@snu.ac.kr

Abstract

In MRI, images of the same contrast (e.g., T1) from the same subject can show noticeable differences when acquired using different hardware, sequences, or scan parameters. These differences in images create a domain gap that needs to be bridged by a step called image harmonization, in order to process the images successfully using conventional or deep learning-based image analysis (e.g., segmentation). Several methods, including deep learning-based approaches, have been proposed to achieve image harmonization. However, they often require datasets of multiple characteristics for deep learning training and may still be unsuccessful when applied to images of an unseen domain. To address this limitation, we propose a novel concept called “Blind Harmonization,” which utilizes only target domain data for training but still has the capability of harmonizing unseen domain images. For the implementation of Blind Harmonization, we developed BlindHarmony using an unconditional flow model trained on target domain data. The harmonized image is optimized to have a correlation with the input source domain image while ensuring that the latent vector of the flow model is close to the center of the Gaussian. BlindHarmony was evaluated using simulated and real datasets and compared with conventional methods. BlindHarmony achieved a noticeable performance in both datasets, highlighting its potential for future use in clinical settings.

1. Introduction

Magnetic resonance imaging (MRI) is a widely-used medical imaging modality. With the advent of deep learning-powered computer vision techniques, there have been numerous applications of deep learning in MRI, such as disease classification [5, 36, 23], tumor segmentation [3, 45], and solving inverse problems [18, 44]. Despite the notable performance of deep learning in MRI, its widespread usage has been hindered by the inherent domain gap present in MRI data [6, 8]. Variations occur in MRI images across

different vendors, scanners, sites, and scan parameters. This domain gap presents a generalization issue when applying the data to a neural network that has been trained on a different dataset.

To overcome the challenges of generalization in deep learning applied to MRI data, several harmonization methods have been developed to match the source domain image to the characteristics of the target domain. These approaches include non-deep learning-based methods [37, 31, 38, 29, 34, 15] and deep learning-based methods [9, 30, 26, 10, 13, 17], which have demonstrated significant performance improvements. However, there are limitations that need to be addressed. Firstly, many of these methods require multiple datasets from different domains. For instance, DeepHarmony which is a supervised end-to-end framework requires “traveling subjects” who undergo multiple MRI scans with different scanners to obtain images from both the source and target domains [9]. The application of CycleGAN-based style transfer can mitigate the need for traveling subjects [30, 26], it still necessitates large datasets with multiple domains. Secondly, the harmonization network trained for mapping between specific source and target domains is challenging to be applied in novel domains, limiting the generalizability of methods. Efforts have been made to adopt a disentanglement approach and domain adaptation to perform harmonization in unseen domains, but it requires a multi-contrast and multi-site paired dataset [10, 47]. To overcome these challenges, we propose the concept of “Blind Harmonization”, where the harmonization network can be constructed only with the target domain data during training and applicable to diverse source domains that are unseen during training.

In recent years, a class of invertible generative models called normalizing flows [11, 21, 12] has been introduced and has shown exceptional performance in a broad range of computer vision tasks. [27, 2, 33] Normalizing flows have a unique capability of not only generating novel images that resemble samples from the distribution of a specific dataset but also mapping the probabilistic distribution of image datasets. This feature makes normalizing flows

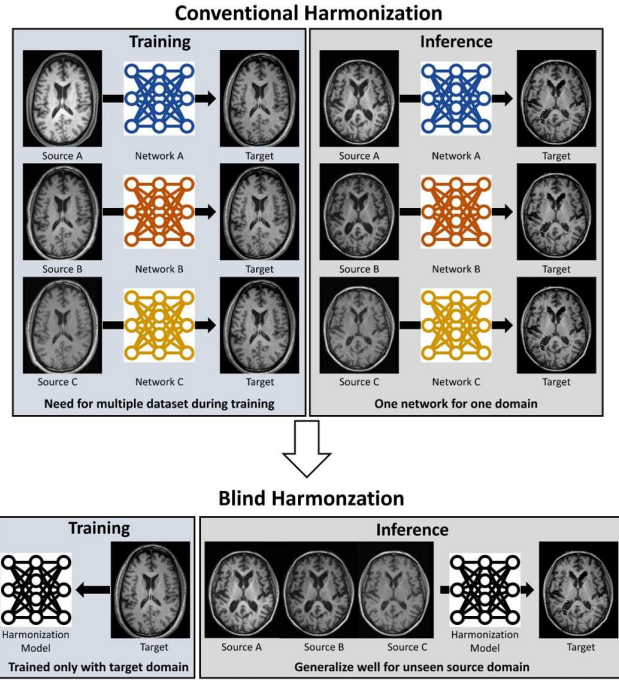


Figure 1. Blind harmonization is a novel approach to address the limitations of conventional harmonization models, which typically require multiple datasets during training or exhibit degraded performance when applied to datasets in unseen domains. By training the model solely with target domain data, blind harmonization can generalize for unseen source domains, and is a novel solution to improve the generalizability of harmonization methods in medical imaging.

particularly well-suited for image generation and manipulation tasks, as they can effectively capture the underlying distribution of image data and generate new images that are consistent with that distribution. Furthermore, the invertibility of these models provides fine-grained control over the generated images, making them useful for tasks such as image editing and style transfer. [1, 41]

In this paper, as a solution for blind harmonization, we introduce BlindHarmony which is a flow-based blind MR image harmonization framework that only utilizes target domain information during training. Our method aims to find the harmonized image that sustains the anatomical structure and contrast of the input image while maintaining a high likelihood in the flow model (*i.e.*, enabling harmonization for the target domain), leveraging the invertibility of flow models. Our contributions are as follows:

1. We present the concept of blind harmonization, which does not require the source domain information during training and perform harmonization for the images of untrained domains.
2. As an implementation of blind harmonization, we pro-

pose BlindHarmony. In BlindHarmony, the flow model is trained solely with the target domain and the harmonized image is optimized by leveraging the invertibility of the flow model.

3. We evaluate our method using both simulated data and real-world data.

2. Related works

2.1. MRI harmonization

There are numerous demands for harmonizing MR images from different sites, vendors, or scanners. Several studies have proposed methods for harmonizing MR images from the source domain to the target domain. Conventionally, these approaches have relied on post-processing techniques at the image level, such as histogram matching [38, 32, 31] and statistical normalization [15, 34, 37], which aims to adjust the intensity values of the images to make them more similar. However, with recent advances in deep learning, there has been growing interest in developing deep learning-based methods for harmonization. One popular deep learning-based method is DeepHarmony [9], which utilizes an end-to-end supervised framework to learn the mapping between the source and target domains. Although DeepHarmony has demonstrated promising results, it requires a large dataset of traveling subjects for training, which can be difficult to acquire. To address this limitation, researchers have employed CycleGAN-based style transfer networks [30, 26]. CycleGAN is a generative adversarial network (GAN) that can learn to map images from one domain to another without the need for paired data. By training CycleGAN on a large dataset of MR images, it is possible to generate images that are visually similar to the target domain while retaining the relevant anatomical features. More recently, researchers have developed separated networks for the contrast network and structure network to enable more flexible applicability. CALAMITI [10, 47] is a GAN-based method that disentangles the contrast and structural information in MR images and allows for more granular control over the image properties that need to be harmonized. In addition to image-level transformations, some works have focused on feature-level harmonization. These methods aim to learn a common feature representation that can be used for downstream analysis tasks. For example, task-based harmonization methods [13, 17] learn a task-specific feature representation that can improve the performance of a specific analysis task.

2.2. Normalizing flow

The flow-based model is a family of generative models, known as normalizing flows, that enables the parametrization of complex data distributions with a series of invertible transformations from simple random variables. In [11], nor-

malizing flows were first introduced, and the NICE model was proposed as a deep learning framework that maps the complex high-dimensional density of training data to a simple factorized space using non-linear bijective transformations. Substantial improvements in invertible neural networks and high-quality image generation from the sample space have been achieved by [21, 12, 11]. In particular, GLOW [21] proposed an efficient and parallelizable transformation using invertible 1×1 convolutions for designing invertible neural networks and demonstrated remarkable results in high-resolution image synthesis tasks. By introducing a log-likelihood-based model in normalizing flows, GLOW can efficiently generate high-resolution natural images. Recent studies have demonstrated great performance of the normalizing flows model in a wide range of computer vision tasks such as super-resolution[27, 39], denoising [2, 27], and colorization [25], using the properties of the normalizing flows model. Among them, SRFLOws [27] adopted negative log-likelihood loss and successfully generated more diverse super-resolution images than GAN-based approaches by conditioning on low-resolution images.

2.3. Prior-based optimization

Conventionally, the inverse problem of $y = Ax$ is widely solved by using regularization techniques. With the advent of generative models, several studies have proposed methods that solve this problem using generative models as prior models or regularizers. Generative adversarial networks (GANs) [7], flow models [4, 43], and deep image priors [40] are commonly used as priors. Individual training of these priors has the benefit of generalizability in the matrix A . For example, in the case of reconstructing MR images from undersampled images, using a generative model prior can be applied to diverse sampling masks [19, 28, 22].

3. Methods

3.1. Harmonization model

When a subject undergoes multiple scans with different vendors or MRI scan parameters, the resulting MR images exhibit differences, mainly in low-frequency, while the structural differences are relatively small. This provides some insight into the relationship between images from different domains. Firstly, the images are highly correlated, as the difference between domains does not significantly impact the overall. Secondly, the edges of the images coincide. Given x_s as the source domain image and x_h as its corresponding harmonized version to the target domain, the following equation holds due to the correlation and edge coincidence:

$$NCC(x_h, x_s) \approx 1 \quad (1)$$

$$M|Gx_h| \approx 0 \quad (2)$$

In these equations, M is a mask obtained by thresholding the gradient value of x_s , which retains only the non-edge regions. G represents the gradient operator, and NCC denotes normalized cross-correlation. Equation 1 suggests that the harmonized image should have a high cross-correlation value with the source domain image. Equation 2 enforces edge sparsity in the harmonized image within regions where the source domain image is considered not to have any edges.

Based on the formulation above, we can define a distance measure, D , between the source domain image and the harmonized image:

$$D(x_h, x_s) = \beta_1 \{1 - NCC(x_h, x_s)\} + \beta_2 M|Gx_h| \quad (3)$$

Here, β s are hyperparameters. However, the problem of finding x_h that satisfies $D(x_h, x_s) = 0$ given x_s is highly ill-posed, as there exists a trivial solution of $x_h = x_s$. Nevertheless, if the prior distribution of the target domain $p_X(x)$ is given, the problem can be solved using a regularization approach:

$$\widehat{x_h} = \arg \min_x D(x, x_s) - \alpha \log p_X(x), \quad (4)$$

where α is a regularization parameter. The remaining issue is how to estimate the prior distribution of the target domain and optimize the solution for $\widehat{x_h}$. We have selected the normalizing flow model to map the distribution of the target domain, as the inherent invertibility of the flow model can provide an advantage for optimization.

3.2. Flow-based prior learning

A normalizing flow is an invertible transformation that maps a sample from a simple probability distribution (such as a normal Gaussian) to a sample from a complex probability distribution. The transformation itself (which is often called “flow”) and its inverse are assumed to be differentiable.

Let $Z \in \mathbb{R}^D$ be a random variable with an associated probability density function (PDF) $p_Z : \mathbb{R}^D \rightarrow [0, 1]$ which is assumed to be known and tractable. Let $f_\theta : \mathbb{R}^D \rightarrow \mathbb{R}^D$ be a diffeomorphism parameterized by the vector $\theta \in \mathbb{R}^P$ with an inverse denoted by f_θ^{-1} . Then the PDF of the random variable $X = f_\theta^{-1}(Z)$ can be computed explicitly using the change of variables formula:

$$p_X(x|\theta) = p_Z(f_\theta(x)) \left| \det \frac{\partial f_\theta(x)}{\partial x} \right|, \quad (5)$$

where $\frac{\partial f_\theta(x)}{\partial x}$ is the Jacobian of f_θ .

When applying normalizing flows for sample generation or density estimation problems, the simple distribution p_Z , known as the “latent distribution”, is transformed via the “flow” f_θ to a more complex distribution p_X . The objective for both problems is to find the value of the parameters

θ for which p_X closely approximates the underlying distribution p_{data} of the given dataset. Only after the objective is satisfied can we accurately estimate densities of random samples using the change of variable formula or generate random samples that are consistent with the given data by first sampling from the latent distribution and feeding the sample to the inverse of the flow.

The aforementioned objective can be stated formally as a maximum likelihood estimation (MLE) problem: maximizing the expected log-likelihood

$$\mathcal{L}(\theta; x) := E_{X \sim p_{data}} [\log(p_X(X|\theta))] \quad (6)$$

$$\approx \frac{1}{N} \sum_{i=1}^N \log \left(p_X \left(x^{(i)} | \theta \right) \right) \quad (7)$$

$$= \frac{1}{N} \sum_{i=1}^N \left[\log \left(p_Z \left(f_\theta \left(x^{(i)} \right) \right) \right) + \log \left| \det \frac{\partial f_\theta(x^{(i)})}{\partial x} \right| \right] \quad (8)$$

over the possible values of the parameters $\theta \in \mathbb{R}^P$, where $\mathcal{D} := \{x^{(i)}\}_{i=1}^N$ is the given dataset. Therefore, training the normalizing flow involves updating the parameters of the flow so that the expected log-likelihood is maximized.

In order to accurately and efficiently approximate the target distribution p_{data} , a normalizing flow f_θ must satisfy several conditions: It must be a bijection with differentiable forward and inverse transformations, it must be expressive enough to model the complexity of the target distribution, and the computations of f_θ , f_θ^{-1} , and $\det \frac{\partial f_\theta(x)}{\partial x}$ must be done efficiently.

Therefore, many state-of-the-art normalizing flows use neural networks that are carefully designed to have differentiable inverse transformations and a Jacobian matrix whose determinant can be calculated efficiently. These include coupling transforms, which have been shown to be particularly effective.

3.3. BlindHarmony optimization

In order to harmonize images from unknown domains, an unconditional flow model is trained solely on the target domain. The prior distribution of the harmonized image x can be parameterized as follows:

$$\log p_X(x) = \log(p_Z(z)) + \log \left| \det \frac{\partial f_\theta(x)}{\partial x} \right| \quad (9)$$

If z is a normal Gaussian, we can rewrite Equation 4 in the z -domain as follows:

$$\hat{z}_h = \arg \min_z D(f_\theta^{-1}(z), x_s) - \alpha \log p_Z(z) \quad (10)$$

$$= \arg \min_z D(f_\theta^{-1}(z), x_s) + \alpha |z|^2 \quad (11)$$

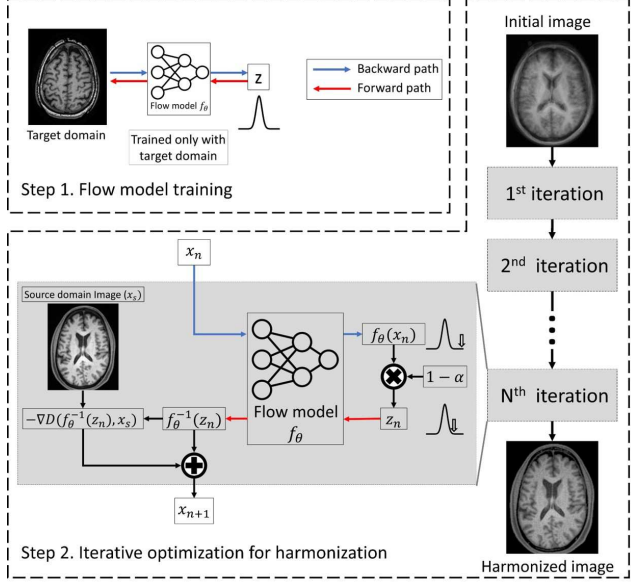


Figure 2. The BlindHarmony framework operates in the following manner: initially, a flow model is trained solely on target domain data to estimate the target domain's prior distribution. Subsequently, source-to-target domain harmonization is performed iteratively by utilizing the trained flow model. The length of the latent variable z is reduced by $(1-\alpha)$, which draws z near to the center of the Gaussian. Gradient descent is employed to ensure that the generated image is not too far away from the source domain image.

The optimization process of Equation 11 requires the calculation of gradients of $f_\theta^{-1}(z)$, which can be computationally burdensome. To increase computational efficiency and reduce processing time, we simply drop the calculation of $\frac{\partial f_\theta^{-1}(z)}{\partial z}$. Instead, iterative optimization is performed in both the z - and x -domains, by leveraging the invertibility of normalizing flow. The algorithm alternates between taking a gradient descent of the distance measure $D(x, x_s)$ and the prior term $|z|^2$.

In the latent vector domain z , z is updated so that it does not deviate far from the center of the Gaussian:

$$z \rightarrow (1 - \alpha)z \quad (12)$$

In the image domain x , the gradient of $D(x, x_s)$ is measured and updated at each iteration as follows:

$$x \rightarrow x + \beta_1 \nabla_x NCC(x, x_s) - \beta_2 \nabla_x M|Gx| \quad (13)$$

After N iterations, the resultant image x is the harmonized image \hat{x}_h . The overall algorithm is formulated as Algorithm 1 and Figure 2. The hyperparameters α , β_1 , and β_2 are found heuristically using grid search. Hyperparameters were fixed as: $\alpha = 0.001$, $\beta_1 = 1000$, $\beta_2 = 0.001$, $N = 10$. The initial image x_0 is selected to be an averaged image of training data images.

Algorithm 1 BlindHarmony optimization

x_s : Source domain image
 \widehat{x}_h : Harmonized image
 f_θ : Flow model trained on the target domain
 x_0 : Initial image
 α, β_1, β_2 : Hyperparameters
 N : The number of iteration

Require: $x_s, x_0, \alpha, \beta_1, \beta_2$

```
1: for  $n = 0, 1, \dots, N - 1$  do
2:    $x_{n+1} = f_\theta(z_n) + \beta_1 \nabla_x NCC(x, x_s)_{x=f_\theta(z_n)} -$ 
    $\beta_2 \nabla_x M|Gx|_{x=f_\theta(z_n)}$ 
3:    $z_{n+1} = (1 - \alpha) f_\theta^{-1}(x_{n+1})$ 
4: end for
5:  $\widehat{x}_h = x_N$ 
```

4. Experiments

4.1. Dataset

The T1-weighted images in the OASIS3 dataset [24] were used to train and evaluate the proposed framework. The OASIS3 dataset consists of images scanned with different scanners. Images acquired with the Siemens Tri-oTim scanner were used as a target domain. For source domain datasets, three datasets consisting of images acquired with other manufacturer models (Domain 1,2,3) and a dataset from a different scanner with the same manufacturer model (Domain 4) were utilized (See Supplementary material). All images were resampled to the same resolution of $1.2 \times 1.2 \times 1.2$ mm and min-max normalized in a slice level.

4.2. Network training detail

In our experiments, we used the Neural Spline Flow (NSF) architecture with rational quadratic (RQ) spline coupling layers that was outlined by [14]. A Glow-like multiscale architecture was used, following NSF (Durkan et al., 2019) and Glow [21]. Each layer of the network contains 7 transformation steps, where each step consists of an actnorm layer, an invertible 1×1 convolution an RQ spline coupling transform, and another 1×1 convolution. The network consists of 4 layers, which results in a total of 28 coupling transformation steps. Also, 3 residual blocks and batch normalization layers are included in the subnetworks parameterizing the RQ splines. An Adam optimizer with an initial learning rate of 0.0005 and cosine annealing of the learning rate was used to iteratively optimize the parameters up to 20K steps. The sampled images are reported in the Supplementary material.

4.3. Simulated data evaluation

To evaluate the effectiveness of our proposed harmonization approach, we developed simulated data by applying

three distinct image transformations: exponential transformation (Domain-Exp), log transformation (Domain-Log), and Gamma transformations with powers of 0.7 (Domain-Gamma0.7) to the target domain images. The target domain images were normalized with min-max normalization, then three transformations above were performed. The min-max normalization was conducted again for the transformed images to generate simulated source domain data. We applied BlindHarmony to the source domain.

To evaluate the performance of our proposed method, we compared it with the following methods: histogram matching (HM), low-frequency replacing (SSIMH) [16], end-to-end U-net [35], and unsupervised CycleGAN [46]. We trained U-net_{Exp}, U-net_{Log}, U-net_{Gamma07} and CycleGAN_{Exp}, CycleGAN_{Log}, CycleGAN_{Gamma07} models for each domain mapping and used them for comparison.

Figure 3 displays the results of our harmonization approach using BlindHarmony on each of the simulated source domain images (1st column), along with the target domain image (2nd column), and the other methods. A visual inspection of the results confirms the effectiveness of our approach in harmonizing images. On the other hand, CycleGAN and U-net fail to harmonize one source domain image when trained on another source domain dataset. In contrast, BlindHarmony offers a more efficient and versatile solution by utilizing a single network for harmonization across diverse source domains.

Table 1 presents the results of our simulated data evaluation of the harmonization methods. We calculated the peak signal-to-noise ratio (PSNR) and structural similarity (SSIM) values using the target image as a reference. The table shows that our proposed BlindHarmony framework outperforms the source domain image, as evidenced by improved PSNR and SSIM values. The PSNR value improved from 21.9 dB for the source domain images to 28.7 dB for the BlindHarmony harmonized image. These results demonstrate the effectiveness of BlindHarmony in harmonizing images from different domains.

It is worth noting that U-net and CycleGAN outperformed BlindHarmony when they were trained separately for each source domain. However, BlindHarmony used and requires only one network for all source domain applications, which makes it a practical solution for harmonizing images from multiple source domains.

4.4. Real-world data application

In addition to the simulation dataset, we also evaluated BlindHarmony on four real datasets from different scanners. We utilized 20 traveling subjects who underwent multi-scanner scans, so we can compare the results quantitatively. The image of each source domain is registered to the target domain image by using FSL FLIRT [20] function. We compared the results with the other methods (U-Net and Cycle-

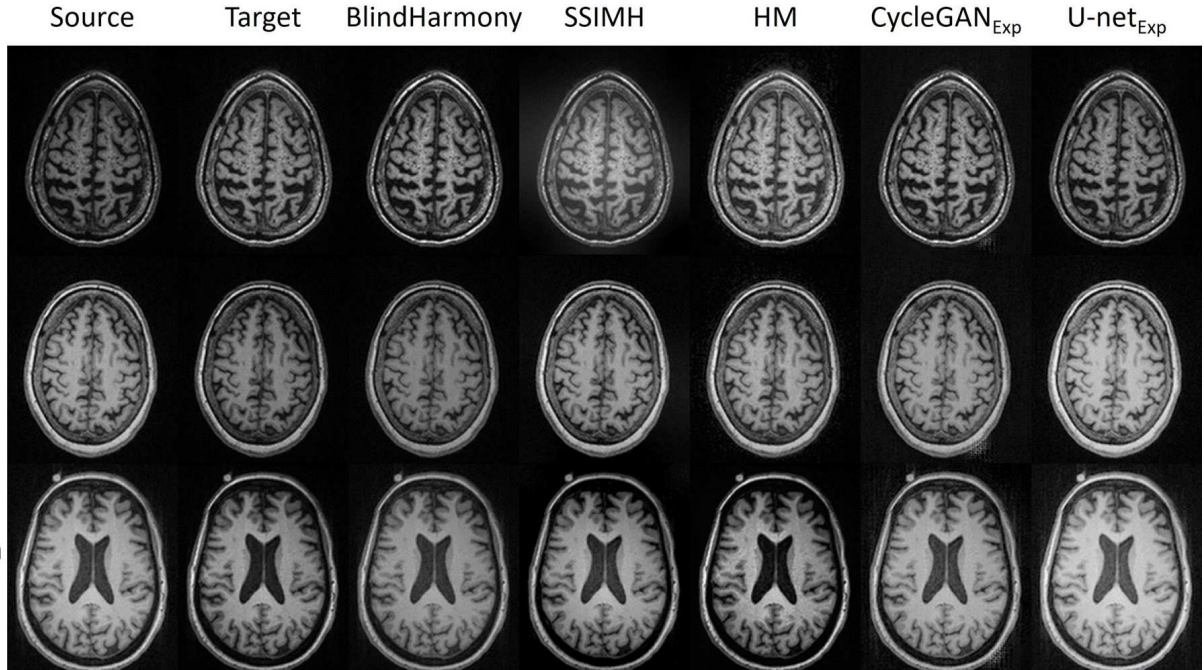


Figure 3. Example image of BlindHarmony application of simulated source domain images and comparison with other harmonization methods.

	Unsupervised	Blind	Exp		Log		Gamma 0.7	
			PSNR(\uparrow)	SSIM(\uparrow)	PSNR(\uparrow)	SSIM(\uparrow)	PSNR(\uparrow)	SSIM (\uparrow)
Source			22.6	0.952	21.4	0.958	21.6	0.955
BlindHarmony (Ours)	O	O	29.7	0.985	28.7	0.979	27.5	0.971
HM	O	O	26.5	0.961	26.5	0.961	26.5	0.961
SSIMH	O	O	26.1	0.971	25.8	0.972	26.2	0.945
CycleGAN _{Exp}	O	X	32.6	0.993	23.0	0.951	22.3	0.948
CycleGAN _{Log}	O	X	22.8	0.943	35.5	0.996	34.5	0.995
CycleGAN _{Gamma07}	O	X	22.1	0.932	35.6	0.996	35.6	0.996
U-net _{Exp}	X	X	65.6	0.999	15.9	0.885	15.9	0.879
U-net _{Log}	X	X	16.8	0.803	56.5	0.999	38.0	0.997
U-net _{Gamma07}	X	X	16.3	0.766	39.2	0.998	55.1	0.999

Table 1. The PSNR and SSIM values calculated between the harmonized image from the simulated source domain and the reference of the target domain image.

GAN retrained for these datasets and conventional methods HM and SSIMH). Figure 4 presents the results of harmonizing the source domain images (column 1) to the target domain images (column 2) using BlindHarmony (column 3). BlindHarmony effectively harmonized the images and reduced the inter-scanner variability, bringing them closer to the target domain images. The BlindHarmony also demonstrated superior harmonization performance than not only the conventional methods (SSIMH, HM) but also the CycleGAN, which illustrates structural distortion.

The quantitative evaluation using the peak signal-to-

noise ratio (PSNR) and structural similarity (SSIM) metrics demonstrated significant improvements in both PSNR and SSIM values compared to the source images (PSNR: 21.5 dB \rightarrow 22.2 dB). In particular, BlindHarmony has exhibited superior metric results compared to the HM, SSIMH, and CycleGAN algorithms, and even outperformed the U-Net in terms of SSIM value.

The effect size of PSNR and SSIM improvement observed in this study is smaller than that in the simulated data study. This can be attributed to two key factors. Firstly, the domain gap between the source and target domains might be

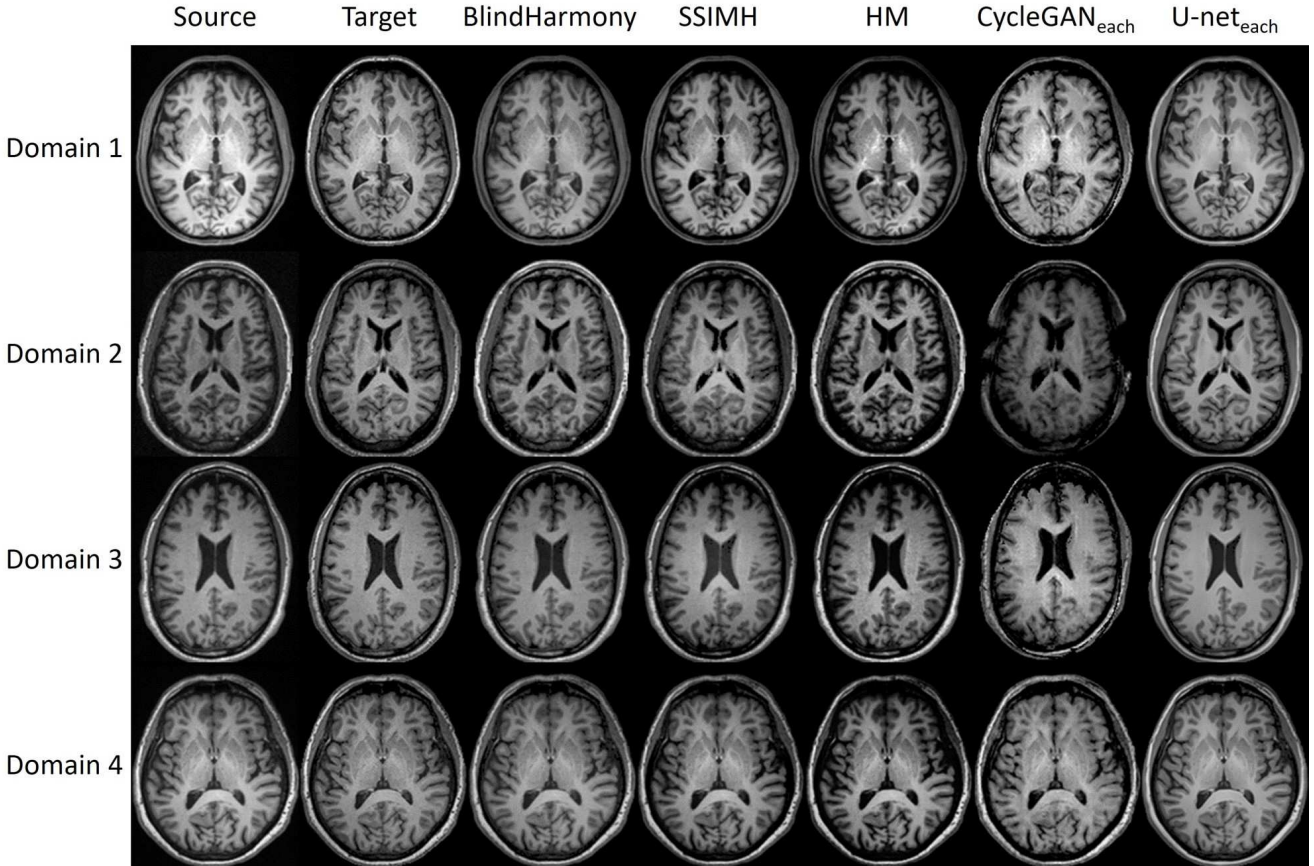


Figure 4. Example image of BlindHarmony application of real source domain images and comparison with other harmonization methods. CycleGAN and U-net results stand for the output of the network that was trained for each source domain.

	Unsupervised	Blind	Domain1		Domain2		Domain3		Domain4	
			PSNR(↑)	SSIM(↑)	PSNR(↑)	SSIM(↑)	PSNR(↑)	SSIM(↑)	PSNR(↑)	SSIM(↑)
Source			19.6	0.833	19.4	0.836	23.0	0.893	24.1	0.914
BlindHarmony	O	O	20.2	0.839	20.8	0.850	23.1	0.893	24.7	0.913
HM	O	O	20.5	0.831	20.7	0.842	22.6	0.884	23.9	0.900
SSIMH	O	O	20.6	0.831	20.4	0.835	22.1	0.883	22.7	0.897
CycleGAN _{each}	O	X	7.22	0.451	6.72	0.447	6.62	0.442	8.62	0.437
U-net _{each}	X	X	25.0	0.919	21.1	0.832	22.2	0.861	21.5	0.879

Table 2. The quantitative results of application to real-world data. PSNR and SSIM values were calculated by using the target domain image as a reference. The case using BlindHarmony illustrated improved consistency to the target domain image.

smaller than that in the simulated data, leading to a weaker harmonization effect. Secondly, the registration process between the source and target domains may not be perfectly aligned due to potential errors in registration and the time gap between separate scans. These factors may have led to the underestimation of the effect of harmonization during metric calculation.

It is important to note that the dataset size used for CycleGAN training was smaller than that used for the flow model training. Additionally, in the case of U-net training,

the dataset size was smaller due to the requirement of paired data. (e.g., Flow model training: 75240 slices, Domain 1 CycleGAN training: 17400 slices, Domain1 U-net training: 5100 slices; See Supplementary materials) Moreover, the construction of paired datasets required registration of the source domain image to the target domain image using the FSL FLIRT function. Despite the efforts, there may still exist misregistration in source domain-target domain pairs, which can negatively affect the training procedure and result in slightly blurred images produced by U-Net. These

may be the reason for the inferior performance of CycleGAN and U-Net compared to their application for simulated source domains.

5. Discussion

We proposed BlindHarmony, a blind harmonization framework for harmonizing MR images from the source domain to the target domain. This framework does not require source domain information and data during training and can be applied to unseen images. The flow-based prior distribution network is trained, and the harmonized images are optimized using a distance between the source domain image and sampled image while using regularization based on the magnitude of the latent vector.

The fact that BlindHarmony does not require source domain information during training is beneficial when applying the neural network to an unknown dataset or a dataset that does not have sufficient data for training. For example, a deep learning-based API provider that utilizes a network trained with a certain dataset may not know the source domain information. In this scenario, our framework can be used as an excellent initial approach that harmonizes data until sufficient data is collected for other methods.

In a real-world dataset evaluation, BlindHarmony demonstrated superior performance compared to CycleGAN and U-net, which were particularly trained for certain source domains. The U-net requires perfectly registered paired datasets of both source and target domains for training, limiting the available dataset size. As for CycleGAN, it was originally developed for transferring style from source to target domains. In this harmonization case, the fine structure in MR images can also be considered as a style from the perspective of CycleGAN, leading to structural distortion in CycleGAN harmonization.

5.1. Limitations

BlindHarmony incorporates iterative optimization in both the image and latent vector domains. In order to reduce the computational burden of calculating the gradient of network parameters, we ignored the determinant term in Equation 9. Although this may compromise mathematical rigor, we believe that this simplification makes calculations easier and reduces processing time, making BlindHarmony more advantageous for practical use.

Additionally, it should be noted that BlindHarmony may not be applicable in every domain. If the distance between two images defined in Equation 3 cannot capture the relationship between images of different domains (*e.g.*, multi-contrast: T1-weighted and T2-weighted images), the optimization may fail and lead to poor results. Therefore, it is important to carefully consider the suitability of BlindHarmony for different applications. For example, when applying the simulated source domain data with Gamma transform-

	Gamma 1.5	
	PSNR(\uparrow)	SSIM(\uparrow)
Source	20.6	0.833
BlindHarmony ($\beta_1 = 1000$)	25.8	0.961
BlindHarmony ($\beta_1 = 500$)	26.8	0.967
HM	26.5	0.961
SSIMH	25.8	0.968

Table 3. Example of failure case. In the case that the source domain is simulated by using the Gamma transformation of 1.5, BlindHarmony produced inferior results when using predefined hyperparameters. However, the results would become better with finetuning of hyperparameters.

mation with a power of 1.5, BlindHarmony showed inferior results to conventional methods. (Table. 3)

However, fine-tuning hyperparameters for each source domain may give improved results. As shown in Table 3, the PSNR and SSIM values increased when we changed the hyperparameter β_1 from 1000 to 500. Tuning these hyperparameters for each source domain may give a successful application of our approach in various scenarios, providing a highly adaptable and versatile solution. Future work may include optimizing these parameters using a transfer learning approach, as demonstrated in [42].

6. Conclusion

In this study, we propose BlindHarmony, a flow-based blind harmonization method for MR images. Unlike other existing harmonization methods, our approach is trained exclusively on the target domain dataset and can be applied to previously unseen domain images. The flow model is trained solely on the target domain data, and the harmonized image is optimized to have correlation with the source domain image while maintaining a high probability of the flow model. Both simulated and real-world datasets found that our method achieved acceptable results. Our study demonstrates the feasibility blind harmonization, providing a significant advantage in scenarios where access to source domain data is limited or unavailable.

References

- [1] Rameen Abdal, Peihao Zhu, Niloy J Mitra, and Peter Wonka. Styleflow: Attribute-conditioned exploration of stylegan-generated images using conditional continuous normalizing flows. *ACM Transactions on Graphics (ToG)*, 40(3):1–21, 2021.
- [2] Abdelrahman Abdelhamed, Marcus A Brubaker, and Michael S Brown. Noise flow: Noise modeling with conditional normalizing flows. In *Proceedings of the IEEE/CVF International Conference on Computer Vision*, pages 3165–3173, 2019.

[3] Zeynettin Akkus, Alfia Galimzianova, Assaf Hoogi, Daniel L Rubin, and Bradley J Erickson. Deep learning for brain mri segmentation: state of the art and future directions. *Journal of digital imaging*, 30:449–459, 2017.

[4] Muhammad Asim, Max Daniels, Oscar Leong, Ali Ahmed, and Paul Hand. Invertible generative models for inverse problems: mitigating representation error and dataset bias. In *International Conference on Machine Learning*, pages 399–409. PMLR, 2020.

[5] Silvia Basaia, Federica Agosta, Luca Wagner, Elisa Canu, Giuseppe Magnani, Roberto Santangelo, Massimo Filippi, Alzheimer’s Disease Neuroimaging Initiative, et al. Automated classification of alzheimer’s disease and mild cognitive impairment using a single mri and deep neural networks. *NeuroImage: Clinical*, 21:101645, 2019.

[6] Viola Biberacher, Paul Schmidt, Anisha Keshavan, Christine C Boucard, Ruthger Righart, Philipp Sämann, Christine Preibisch, Daniel Fröbel, Lilian Aly, Bernhard Hemmer, et al. Intra-and interscanner variability of magnetic resonance imaging based volumetry in multiple sclerosis. *NeuroImage*, 142:188–197, 2016.

[7] Ashish Bora, Ajil Jalal, Eric Price, and Alexandros G Dimakis. Compressed sensing using generative models. In *International Conference on Machine Learning*, pages 537–546. PMLR, 2017.

[8] Kristi A Clark, Roger P Woods, David A Rottenberg, Arthur W Toga, and John C Mazziotta. Impact of acquisition protocols and processing streams on tissue segmentation of t1 weighted mr images. *NeuroImage*, 29(1):185–202, 2006.

[9] Blake E Dewey, Can Zhao, Jacob C Reinhold, Aaron Carass, Kathryn C Fitzgerald, Elias S Sotirchos, Shiv Saidha, Jiwon Oh, Dzung L Pham, Peter A Calabresi, et al. Deepharmony: A deep learning approach to contrast harmonization across scanner changes. *Magnetic resonance imaging*, 64:160–170, 2019.

[10] Blake E Dewey, Lianrui Zuo, Aaron Carass, Yufan He, Yihao Liu, Ellen M Mowry, Scott Newsome, Jiwon Oh, Peter A Calabresi, and Jerry L Prince. A disentangled latent space for cross-site mri harmonization. In *Medical Image Computing and Computer Assisted Intervention–MICCAI 2020: 23rd International Conference, Lima, Peru, October 4–8, 2020, Proceedings, Part VII*, pages 720–729. Springer, 2020.

[11] Laurent Dinh, David Krueger, and Yoshua Bengio. Nice: Non-linear independent components estimation. *arXiv preprint arXiv:1410.8516*, 2014.

[12] Laurent Dinh, Jascha Sohl-Dickstein, and Samy Bengio. Density estimation using real nvp. *arXiv preprint arXiv:1605.08803*, 2016.

[13] Nicola K Dinsdale, Mark Jenkinson, and Ana IL Namburete. Deep learning-based unlearning of dataset bias for mri harmonisation and confound removal. *NeuroImage*, 228:117689, 2021.

[14] Conor Durkan, Artur Bekasov, Iain Murray, and George Papamakarios. Neural spline flows. *Advances in neural information processing systems*, 32, 2019.

[15] Jean-Philippe Fortin, Drew Parker, Birkan Tunç, Takanori Watanabe, Mark A Elliott, Kosha Ruparel, David R Roalf, Theodore D Satterthwaite, Ruben C Gur, Raquel E Gur, et al. Harmonization of multi-site diffusion tensor imaging data. *Neuroimage*, 161:149–170, 2017.

[16] Hao Guan, Siyuan Liu, Weili Lin, Pew-Thian Yap, and Mingxia Liu. Fast image-level mri harmonization via spectrum analysis. In *Machine Learning in Medical Imaging: 13th International Workshop, MLMI 2022, Held in Conjunction with MICCAI 2022, Singapore, September 18, 2022, Proceedings*, pages 201–209. Springer, 2022.

[17] Hao Guan, Yunbi Liu, Erkun Yang, Pew-Thian Yap, Dinggang Shen, and Mingxia Liu. Multi-site mri harmonization via attention-guided deep domain adaptation for brain disorder identification. *Medical image analysis*, 71:102076, 2021.

[18] Kerstin Hammernik, Teresa Klatzer, Erich Kobler, Michael P Recht, Daniel K Sodickson, Thomas Pock, and Florian Knoll. Learning a variational network for reconstruction of accelerated mri data. *Magnetic resonance in medicine*, 79(6):3055–3071, 2018.

[19] Ajil Jalal, Marius Arvinte, Giannis Daras, Eric Price, Alexandros G Dimakis, and Jon Tamir. Robust compressed sensing mri with deep generative priors. *Advances in Neural Information Processing Systems*, 34:14938–14954, 2021.

[20] Mark Jenkinson, Peter Bannister, Michael Brady, and Stephen Smith. Improved optimization for the robust and accurate linear registration and motion correction of brain images. *NeuroImage*, 17(2):825–841, 2002.

[21] Durk P Kingma and Prafulla Dhariwal. Glow: Generative flow with invertible 1x1 convolutions. *Advances in neural information processing systems*, 31, 2018.

[22] Yilmaz Korkmaz, Salman UH Dar, Mahmut Yurt, Muzaffer Özbeý, and Tolga Cukur. Unsupervised mri reconstruction via zero-shot learned adversarial transformers. *IEEE Transactions on Medical Imaging*, 41(7):1747–1763, 2022.

[23] Sergey Korolev, Amir Saifullin, Mikhail Belyaev, and Yulia Dodonova. Residual and plain convolutional neural networks for 3d brain mri classification. In *2017 IEEE 14th international symposium on biomedical imaging (ISBI 2017)*, pages 835–838. IEEE, 2017.

[24] Pamela J LaMontagne, Tammie LS Benzinger, John C Morris, Sarah Keefe, Russ Hornbeck, Chengjie Xiong, Elizabeth Grant, Jason Hassenstab, Krista Moulder, Andrei G Vlassenko, et al. Oasis-3: longitudinal neuroimaging, clinical, and cognitive dataset for normal aging and alzheimer disease. *MedRxiv*, pages 2019–12, 2019.

[25] Yuan-kui Li, Yun-Hsuan Lien, and Yu-Shuen Wang. Style-structure disentangled features and normalizing flows for diverse icon colorization. In *Proceedings of the IEEE/CVF Conference on Computer Vision and Pattern Recognition*, pages 11244–11253, 2022.

[26] Mengting Liu, Piyush Maiti, Sophia Thomopoulos, Alyssa Zhu, Yaqiong Chai, Hosung Kim, and Neda Jahanshad. Style transfer using generative adversarial networks for multi-site mri harmonization. In *Medical Image Computing and Computer Assisted Intervention–MICCAI 2021: 24th International Conference, Strasbourg, France, September 27–October 1, 2021, Proceedings, Part III 24*, pages 313–322. Springer, 2021.

[27] Andreas Lugmayr, Martin Danelljan, Luc Van Gool, and Radu Timofte. Srflow: Learning the super-resolution space with normalizing flow. In *Computer Vision–ECCV 2020: 16th European Conference, Glasgow, UK, August 23–28, 2020, Proceedings, Part V 16*, pages 715–732. Springer, 2020.

[28] Guanxiong Luo, Na Zhao, Wenhao Jiang, Edward S Hui, and Peng Cao. Mri reconstruction using deep bayesian estimation. *Magnetic resonance in medicine*, 84(4):2246–2261, 2020.

[29] Hengameh Mirzaalian, Lipeng Ning, Peter Savadjiev, Ofer Pasternak, Sylvain Bouix, O Michailovich, Gerald Grant, Christine E Marx, Rajendra A Morey, Laura A Flashman, et al. Inter-site and inter-scanner diffusion mri data harmonization. *NeuroImage*, 135:311–323, 2016.

[30] Gourav Modanwal, Adithya Vellal, Mateusz Buda, and Maciej A Mazurowski. Mri image harmonization using cycle-consistent generative adversarial network. In *Medical Imaging 2020: Computer-Aided Diagnosis*, volume 11314, pages 259–264. SPIE, 2020.

[31] László G Nyúl and Jayaram K Udupa. On standardizing the mr image intensity scale. *Magnetic Resonance in Medicine: An Official Journal of the International Society for Magnetic Resonance in Medicine*, 42(6):1072–1081, 1999.

[32] László G Nyúl, Jayaram K Udupa, and Xuan Zhang. New variants of a method of mri scale standardization. *IEEE transactions on medical imaging*, 19(2):143–150, 2000.

[33] George Papamakarios, Eric Nalisnick, Danilo Jimenez Rezende, Shakir Mohamed, and Balaji Lakshminarayanan. Normalizing flows for probabilistic modeling and inference. *The Journal of Machine Learning Research*, 22(1):2617–2680, 2021.

[34] Raymond Pomponio, Guray Erus, Mohamad Habes, Jimit Doshi, Dhivya Srinivasan, Elizabeth Mamourian, Vishnu Bashyam, Ilya M Nasrallah, Theodore D Satterthwaite, Yong Fan, et al. Harmonization of large mri datasets for the analysis of brain imaging patterns throughout the lifespan. *NeuroImage*, 208:116450, 2020.

[35] Olaf Ronneberger, Philipp Fischer, and Thomas Brox. U-net: Convolutional networks for biomedical image segmentation. In *Medical Image Computing and Computer-Assisted Intervention–MICCAI 2015: 18th International Conference, Munich, Germany, October 5–9, 2015, Proceedings, Part III 18*, pages 234–241. Springer, 2015.

[36] Christian Salvatore, Antonio Cerasa, Isabella Castiglioni, F Gallivanone, A Augimeri, M Lopez, G Arabia, M Morelli, MC Gilardi, and A Quattrone. Machine learning on brain mri data for differential diagnosis of parkinson’s disease and progressive supranuclear palsy. *Journal of neuroscience methods*, 222:230–237, 2014.

[37] Russell T Shinohara, Jiwon Oh, Govind Nair, Peter A Calabresi, Christos Davatzikos, Jimit Doshi, Roland G Henry, Gloria Kim, Kristin A Linn, Nico Papinutto, et al. Volumetric analysis from a harmonized multisite brain mri study of a single subject with multiple sclerosis. *American Journal of Neuroradiology*, 38(8):1501–1509, 2017.

[38] Russell T Shinohara, Elizabeth M Sweeney, Jeff Goldsmith, Navid Shiee, Farrah J Mateen, Peter A Calabresi, Samson Jarso, Dzung L Pham, Daniel S Reich, Ciprian M Crainiceanu, et al. Statistical normalization techniques for magnetic resonance imaging. *NeuroImage: Clinical*, 6:9–19, 2014.

[39] Ki-Ung Song, Dongseok Shim, Kang-wook Kim, Jae-young Lee, and Younggeun Kim. Fs-ncsr: Increasing diversity of the super-resolution space via frequency separation and noise-conditioned normalizing flow. In *2022 IEEE/CVF Conference on Computer Vision and Pattern Recognition Workshops (CVPRW)*, pages 967–976. IEEE, 2022.

[40] Dmitry Ulyanov, Andrea Vedaldi, and Victor Lempitsky. Deep image prior. In *Proceedings of the IEEE conference on computer vision and pattern recognition*, pages 9446–9454, 2018.

[41] Ben Usman, Avneesh Sud, Nick Dufour, and Kate Saenko. Log-likelihood ratio minimizing flows: Towards robust and quantifiable neural distribution alignment. *Advances in Neural Information Processing Systems*, 33:21118–21129, 2020.

[42] Xinyi Wei, Hans van Gorp, Lizeth Gonzalez-Carabarin, Daniel Freedman, Yonina C Eldar, and Ruud JG van Sloun. Deep unfolding with normalizing flow priors for inverse problems. *IEEE Transactions on Signal Processing*, 70:2962–2971, 2022.

[43] Jay Whang, Qi Lei, and Alex Dimakis. Solving inverse problems with a flow-based noise model. In *International Conference on Machine Learning*, pages 11146–11157. PMLR, 2021.

[44] Jaeyeon Yoon, Enhao Gong, Itthi Chatnuntawech, Berkin Bilgic, Jingu Lee, Woojin Jung, Jingyu Ko, Hosan Jung, Kawin Setsompop, Greg Zaharchuk, et al. Quantitative susceptibility mapping using deep neural network: Qsmnet. *Neuroimage*, 179:199–206, 2018.

[45] Xiaomei Zhao, Yihong Wu, Guidong Song, Zhenye Li, Yazhuo Zhang, and Yong Fan. A deep learning model integrating fcnns and crfs for brain tumor segmentation. *Medical image analysis*, 43:98–111, 2018.

[46] Jun-Yan Zhu, Taesung Park, Phillip Isola, and Alexei A Efros. Unpaired image-to-image translation using cycle-consistent adversarial networks. In *Proceedings of the IEEE international conference on computer vision*, pages 2223–2232, 2017.

[47] Lianrui Zuo, Blake E Dewey, Yihao Liu, Yufan He, Scott D Newsome, Ellen M Mowry, Susan M Resnick, Jerry L Prince, and Aaron Carass. Unsupervised mr harmonization by learning disentangled representations using information bottleneck theory. *NeuroImage*, 243:118569, 2021.